Physica D 60 (1992) 70–83
North-Holland

PHYSICA D

Computations of multi-fluid flows

S. Ozen Unverdi and Grétar Tryggvason [1]
Department of Mechanical Engineering and Applied Mechanics,
2250 G.G. Brown, The University of Michigan, Ann Arbor, MI 48109, USA

Full numerical simulations of three-dimensional flows of two or more immiscible fluids of different densities and viscosities separated by a sharp interface with finite surface tension are discussed. The method used is based on a finite difference approximation of the full Navier–Stokes equations and explicit tracking of the interface between the fluids. Preliminary simulations of the Rayleigh–Taylor instability and the motion of bubbles are shown.

1. Introduction

The considerable recent progress in understanding complex single-phase flows can be attributed to the development of experimental techniques that allow clear visualization of fluid structures (such as LIF) and detailed velocity measurements, and numerical methods that allow simulations of realistic (although simple) unsteady, fully three-dimensional flows. For flows that consist of two (or more) phases, formidable difficulties are still encountered in both experimental and numerical work. The difficulty in penetrating the flow field visually limits the experimental observations (although ingenious techniques have been developed in special circumstances), while on the numerical side, the difficulties associated with the advection of interfaces between two dissimilar fluids have limited studies to simple cases.

Multi-fluid systems are of considerable importance for a large number of natural and technological processes. A list of just a few applications includes spray combustion, boiling, air stripping of contaminants, evaporative cooling, air-lift pumps, blending, mixing and emulsification. Many of these phenomena involve fluids undergoing phase change, but frequently the rate of phase change is smaller than the hydrodynamic time scale; the phase change can therefore be neglected for transient processes such as bubble breakup. However, even such "simple" processes (without phase change) are still poorly understood. Since it is frequently the microscopic structure of a two-fluid mixture (such as the size and density of droplets in a fuel spray) that determines the overall property of interest (e.g. how fast a spray burns), it is important to account accurately for the evolution at the smallest scales. In some cases, in particular when one fluid is dispersed in another one in small drops or bubbles, it is possible to assume that, although the dispersed fluid has a dynamic of its own, the motion of the ambient fluid is minimally affected, see [1] for discussion of such "active microstructures". In most cases, however, the motion of both fluids is coupled, and in some cases the fluid motion itself is induced solely by the fact that the fluids have different properties.

To fully understand the behavior of a multi-fluid system one must have a good insight into the basic micromechanisms that govern the evolution of a single structure (e.g., a bubble or a drop) and the interactions of a few such structures. In addition to the usual questions about the relative magnitude of the various physical ef-

[1] E-mail address: gretar@caen.engin.umich.edu.

fects (inertia, viscosity and surface tension), the effects of surface phenomena such as contaminants must be addressed for multi-fluid systems. Full numerical simulations are, in principle, ideally suited to provide this information. Not only are all the quantitative data readily available, but various physical processes can be turned on and off at will. In practice, however, simulations of multi-fluid problems are one of the difficult areas of computational fluid dynamics. Almost all current studies of multi-fluid problems make a number of simplifications, such as inviscidness, Stokes flow, two-dimensionality or axisymmetry. Although such models capture some of the important behavior, they often put severe constraints on the problems that can be investigated. Many of the fundamental processes in multi-fluid flow are fully three-dimensional, and both inertia and viscous effects must be accounted for.

We have recently developed a front-tracking method for multi-fluid, incompressible flows that appears to be both accurate and robust [2]. The method has been implemented for two- as well as fully three-dimensional situations. In this paper we discuss the method briefly and present preliminary results for the Rayleigh–Taylor instability and the collision of two bubbles.

For fluid mixing induced by unstable stratification, the Rayleigh–Taylor instability, where a heavy fluid falls into a lighter underlying fluid, is the classical example. Indeed, for such flows, its importance is similar to that of the Kelvin–Helmholtz instability for fluid mixing induced by a shear flow. The Rayleigh–Taylor instability has been a prototype problem for computational studies of multi-fluid flows. The early calculations by Daly [3] using the well-known Marker-And-Cell (MAC) method examined the effect of stratification and set the stage for future work. A review of the literature with particular attention to numerical work is given by Sharp [4], and a brief review also appears in [5], which presents inviscid simulations for various density ratios. Other recent inviscid simulations include [6] for the single fluid case and [7] for finite density differences. Boundary integral simulations of a two-dimensional Rayleigh–Taylor instability in the Stokes flow limit, with fluids of identical viscosities are presented by Yiantsios and Higgins [8]. Calculations of the Rayleigh–Taylor instability for inviscid, compressible fluids neglecting surface tension have been done by Glimm et. al. [9] using a two-dimensional front tracking technique and by Youngs [10], who recently calculated the full three-dimensional evolution of a multi-mode perturbation to large amplitude.

For many multi-fluid, mixing problems, the final state consists of drops or bubbles of one phase dispersed in another phase. The motion of drops and bubbles is therefore of a fundamental importance in many mixing processes. Introduction to the subject can be found in the book by Clift, Grace and Weber [11], who discuss the motion of a single bubble, drop and particle in considerable detail. Churchill [12] devotes a chapter to this subject, and several sections in various handbooks (e.g., [13]) contain discussions of the problem. The review by Harper [14] also gives a broad overview of the motion of single drops and bubbles. Reviews of more limited aspects are given by Wegener and Parlange [15] who discuss spherical-cap bubbles and by Rallison [16], who presents an overview of the deformation of small viscous drops and bubbles. This latter topic is also reviewed by Acrivos [17]. Computational studies have been limited, nearly exclusively, to the motion of a single bubble or a drop. For drops and bubbles at zero Reynolds number (Stokes flow) in a strain field, several investigators have applied boundary integral techniques to predict the deformation. Youngren and Acrivos [18] considered a gas bubble in viscous extensional flow, and Rallison [19] considered the time-dependent deformation of a non-axisymmetric drop with a viscosity equal to the surrounding fluid. More recent work includes Stone and Leal's [20] study of the breakup of extended drops and an investigation of the deformation of an initially non-

spherical drop by Koh and Leal [21] and Posrikidis [22]. The last studies show that the spherical shape solution of Hadamart is indeed very stable, but the relaxation toward that shape includes some rather remarkable processes, including the shedding of the fluid in the drop and, in other cases, engulfment of the outer fluid. Chi and Leal [23] studied the axisymmetric motion of a viscous drop toward a fluid interface for a range of capillary numbers and viscosity ratios, and Martinez and Udell [24] considered the motion of drops through circular tubes. Stone and Leal [25] recently investigated the influence of contaminants on the breakup of drops in an axisymmetric strain field.

For non-zero Reynolds numbers, a rising bubble can deform considerably. Ryskin and Leal [26] examined the steady-state shape of a rising axisymmetric bubble for a range of Reynolds and Weber numbers using a finite difference technique and boundary-fitted coordinate system. They also applied their numerical technique to investigate the steady-state shape of bubbles in an axisymmetric strain flow. Dandy and Leal [27] extended the method to the full two-fluid problem where the internal motion of the bubbles is calculated. Recent numerical calculations of the initial deformation of two-dimensional inviscid bubbles include [28] for the case where the density ratio is very small and [29] for the case of a bubble of zero density. Unsteady, two-dimensional flow calculations around deformable drops have been presented by Fyfe, Oran and Fritts [30], who used a moving triangular grid. Inviscid calculations of fully three-dimensional bubbles for weakly stratified flows and excluding surface tension were presented by Brecht and Ferrante [31]. More advanced three-dimensional, inviscid calculations taking the bubble fluid to have zero density and including surface tension have recently been presented by Chahine and coworkers [32]. They have also extended their method to bubbles in an external, rotational flows, where the bubble-induced flow remains irrotational.

For more complicated problems such as bubble/bubble interactions and bubbles in vortical flows where the assumption of a linear flow field is not valid, the literature is mostly confined to experimental studies and analytical models usually based on rather far reaching simplifications. A number of workers have modeled such bubbles by assuming inviscid flow and zero surface tension. The bubble is then essentially a dipole, and the interactions can be approximated by assuming that the velocity of each bubble is its own self-induced velocity plus the contribution from the other dipoles (bubbles). Many of these bubble interaction and coalescence studies have been motivated by bubbling fluidized beds. For a review of analytical modeling, see [33]. For experimental studies on bubble coalescence, see, for example, [34].

2. Formulation and numerical method

Sharp interfaces or fronts separating two relatively smooth flow regions appear in a wide variety of physical situation. Examples include shocks in compressible flows, vortex sheets, or slip lines, in high Reynolds number flows, and interfaces separating different fluids or phases in multi-fluid flows. Although fronts generally have an internal structure, it is frequently possible to approximate them as a surface where some properties of the flow or fluid changes discontinuously. When present, fronts are often the most dominant feature of the flow, and it is essential to predict their movement accurately. However, simulations of flows with fronts are a difficult problem.

Numerical methods specially designed to handle flows containing sharp fronts can be classified into two main categories: front tracking and front capturing. In front tracking methods, the front is treated as a moving internal boundary, and separate grids, aligned with the interface, are used to calculate the smooth solution on either side of the front. The motion of the boundary is

calculated as a part of the solution, using the appropriate boundary conditions across the interface. Often, only the grid in the vicinity of the interface is aligned with the interface, and in general it is necessary to introduce a separate data structure to keep track of the moving interface. In front capturing, on the other hand, no additional information is used to identify the position of the interface. The front appears directly on a fixed grid as a region of steep gradient. Although the front is not treated separately from the rest of the flow, in most cases it is necessary to build operations into the algorithm that are effective only in the front regions. The reason is that classical schemes either lead to excessive diffusion of the jump if the method is of low order (first) or lead to oscillations for higher order methods. To keep the interface sharp, but without oscillations, the basic scheme is usually modified to provide a monotonic, but relatively sharp, interface. The introduction of artificial viscosity is the traditional method, but in the last decade several sophisticated methods have been introduced to achieve the desired result. For a recent review, see [35]. Generally, these methods do well for shocks but less well for material interfaces.

In integral form, the Navier–Stokes equations apply to any flow field, irrespective of whether it contains discontinuities or not. The integral properties of the equations are preserved if the so-called conservative form is discretized by conventional finite difference approximations (alternatively, finite volume methods work with the integral form directly). When the governing equations are written for the whole domain, forces concentrated on the interface, such as surface tension forces, have to be introduced as body forces multiplied by a delta function that is non-zero only on the interface. With this modification, the Navier–Stokes equations are

$$\frac{\partial}{\partial t}(\rho \boldsymbol{u}) + \nabla \cdot (\rho \boldsymbol{u}\boldsymbol{u}) = -\nabla p + \rho \boldsymbol{g} + \nabla \cdot \mu(\nabla \boldsymbol{u} + \nabla \boldsymbol{u}^T) + \sigma \kappa \boldsymbol{n} \delta(\boldsymbol{x} - \boldsymbol{x}^f). \tag{1}$$

Here $\boldsymbol{x}^f$ denotes the position of the front, ρ and μ are the discontinuous density and viscosity fields, respectively, κ is twice the mean interface curvature, and other symbols follow customary convention. These equations are supplemented by the incompressibility condition

$$\nabla \cdot \boldsymbol{u} = 0, \tag{2}$$

which, when combined with eq. (1), leads to an elliptic equation for the pressure. In general the pressure equation is non-separable for flows with non-uniform density, but if the Boussinesq approximation is applicable (weak stratification), a simple Poisson equation for the pressure is obtained. In addition to (1) and (2), equations of state for the material properties are needed. For immiscible, incompressible fluids, these state that the properties of each fluid particle remain constant, or

$$\frac{\partial \rho}{\partial t} + \boldsymbol{u} \cdot \nabla \rho = 0,$$
$$\frac{\partial \mu}{\partial t} + \boldsymbol{u} \cdot \nabla \mu = 0. \tag{3}$$

Here we have used the non-conservative form of these equations to emphasize that this is just the material derivative. In any case, in the method described below, the last two equations are not solved directly, but the fluid properties constructed from the tracked interface.

The front tracking method is described in detail in [2] and only a brief outline is given here. The method is best described as a hybrid between a front tracking and a front capturing method. The interface between the two fluids is tracked explicitly by additional computational elements to advance the density (and viscosity) field, but the flow field is advanced with conservative differences, as in capturing methods,

without any special treatment for the interface, except that surface tension forces are calculated using the interface position. To provide stability and smoothness the interface is not kept completely sharp but is given a finite thickness of the order of the mesh size. This thickness remains constant for all time (no "numerical diffusion") but decreases with finer resolution. Since our fluids are incompressible, the interface simply moves with the fluid velocity, which is interpolated from the grid.

In our implementation, the computations proceed through the following steps: Given a velocity, density and viscosity at time t, the interface is advected to a new position at time $t + \Delta t$. The new density and viscosity field, corresponding to this new interface position is found as described below. The pressure is found by solving an elliptic equation given the velocity at t and the density at both the old and the new times. The pressure and the old velocity and viscosity, along with the density at both the new and the old times are then used to predict the velocity at the new time. Except for the update of the property fields, this procedure is exactly the MAC method (when a staggered grid is used) developed at Los Alamos [3] and described in standard textbooks. The method, as described here, is second order in space but only first order in time. We have implemented a second order version as a predictor-corrector for some of our two-dimensional calculations. However, it is generally necessary to take a very small time step to maintain stability, and in those cases where we have compared the results the second order method offers only a small improvement. Since the first order method is faster, we have used that in our three-dimensional calculations. When calculations are carried out for a long time, it is likely that a higher order method is required to reduce error accumulation.

Methods that incorporate the basic features of our interface treatment are not completely new. The motivation for the present approach comes from the work of one of the authors (G.T.) using a Vortex-In-Cell method to simulate inviscid vortical flows with moving internal boundaries [5] and the work of C.S. Peskin and collaborators, who have simulated a number of viscous flows with moving internal boundaries using a front-tracking technique based on ideas somewhat similar to those used in the Vortex-In-Cell method [36]. In both cases, a moving interface is combined with a fixed grid by distributing the quantity carried by the interface (vorticity in the Vortex-In-Cell method; forces in Peskin's calculations) onto the grid at each time step – creating a smooth field – and then moving the interface with a velocity interpolated from the grid.

The major difference with the new method is that the tracked interfaces carry the jump (or gradient) in properties across the interface. At each time step, the property field is reconstructed by distributing this jump onto the grid, taking the numerical divergence of the resulting gradient field, and then solving a Poisson equation for the density (or the viscosity) by a fast Poisson solver. The primary advantage of this approach is that interfaces can interact in a rather natural way, since the gradients simply add, or cancel, as the grid distribution is constructed from the information carried by the tracked front. This interaction, which is automatically taken care of in our method, is considered one of the great difficulties of front-tracking methods [37].

A major complication with front tracking in three dimensions is the modification of the interface grid, necessary to retain sufficient resolution as the interface stretches and deform. In two dimensions, the front is simply a line, and these modifications are a relatively simple matter. But, when the interface becomes a surface embedded in a three-dimensional flow, this aspect takes on a whole new dimension (literally). The regriding problem is, of course, closely linked to the data structure used to represent the front. We currently represent the surface by triangular elements and use a standard finite element data structure to represent the nodal

points and the elements that link them. The regriding can be divided into several steps, such as node addition, node deletion, and reconnection or restructuring. Our current implementation includes point insertion (for elements that become too large), point removal, and restructuring (to eliminate bad "aspect ratios," i.e., elements with small area but large perimeter). An additional complication is the calculation of the mean surface curvature, which is needed for the surface tension forces. We are currently using a method described by Todd and McLeod [38], modified slightly for our grid structure, that works well in most cases.

3. Results

In this section we show a few preliminary results for two- and three-dimensional simulations of the Rayleigh–Taylor instability and bubble motion. Other results have been reported elsewhere, i.e; a brief discussion of the effect of three-dimensionality on the weakly stratified Rayleigh–Taylor instability is given by Tryggvason and Unverdi [39] and several examples of two- and three-dimensional bubble motion for various density and viscosity ratios, as well as different surface tension values, are shown in [2].

In fig. 1 we show how our method predicts the evolution of a two-dimensional Rayleigh–Taylor instability for three different density ratios. The behavior exhibited is well known. For weak stratification (top row), the interface rolls up near the original position of the interface, and the evolution is nearly symmetric with the up-going bubble looking the same as the down-going spike. For stronger stratification (middle row), the rollup is less and takes place closer to the spike. For even stronger stratification (bottom row), the rollup is almost completely suppressed, and the heavy fluid falls down in a thin spike, but the light fluid rises in a round bubble. In the limit of the single fluid case (where the light fluid has zero density), the bubble rises with constant velocity whereas the spike is in free fall. These results agree with what has been calculated by several other methods, using both the full Navier–Stokes equations or assuming inviscid fluids [3,5]. The major difference from inviscid calculations is that the rollup for the weakly stratified case is greatly reduced. Here, where the viscosity corresponds to the most unstable wavelength, the interface folds over just once. Inviscid calculations predict, on the other

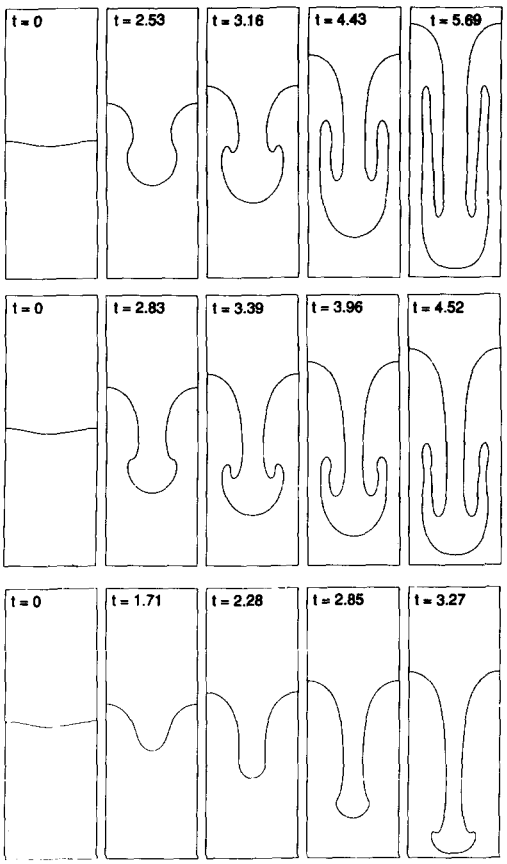

Fig. 1. The effect of density stratification on two-dimensional Rayleigh–Taylor instability. Time sequence for three different density ratios. The Attwood number, $A = (\rho_h - \rho_\ell)/(\rho_h + \rho_\ell)$, is: 0.1 in the top row, 0.5 in the middle row, and 0.9 in the bottom row. The kinematic viscosity of both fluids is the same in all runs and corresponds to the most unstable wave. The non-dimensional time, $t\sqrt{Ag/L}$, is given in each frame. The amplitude of the initial perturbation is 5% of the period length L.

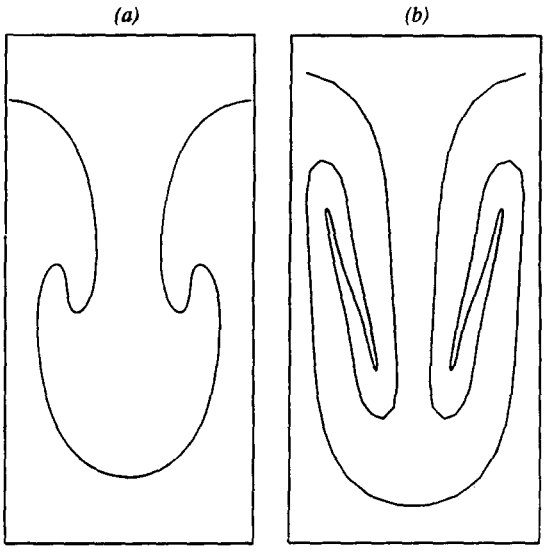

Fig. 2. The effect of viscosity on weakly stratified, two-dimensional Rayleigh–Taylor instability. In (a), the viscosity corresponds to the most unstable wave but in (b), the viscosity is one tenth of that. The non-dimensional time, $t\sqrt{Ag/L}$, is 2.5. The amplitude of the initial perturbation is 10% of the period length L.

hand, the formation of a well-developed vortex. To investigate the effect of viscosity in slightly more detail, we show, in fig. 2a, the evolution of weakly stratified Rayleigh–Taylor instability for the same viscosity as in the top row in fig. 1 (this calculation incorporates the Boussinesq approximation; the run in 1 does not) and a ten times smaller viscosity in 2b. This reduction in viscosity causes the interface to fold over once more, but then the arms appear to undergo similar stretching as in the top frames. This suggests that as the viscosity is decreased for a given perturbation, more rollup would be observed.

Although most computations of the Rayleigh–Taylor instability have assumed two-dimensional evolution, there is – unlike, say, the Kelvin–Helmholtz instability – no stage at which the evolution is predominantly two-dimensional. Even when the experimental setup is "two-dimensional," such as when the flow is confined to a narrow space between parallel walls, the growth of boundary layers at the walls induces three-dimensional motion. It is therefore of considerable importance to consider three-dimensionality in simulations of the Rayleigh–Taylor instability. Fig. 3 shows two calculations of a fully three-dimensional flow. In the top frame, the density of the heavier fluid is three times that of the lighter one, and in the bottom frame, the heavier fluid is twenty times denser than the lighter one. Only one large amplitude stage is shown for each run. To make the structure of the interface a little clearer, we actually show two periods, although only one was simulated. In these runs, the interface surface tension is taken as zero, and the interface grid has not been restructured. For small density stratification, we have shown [39] that three-dimensionality can lead to a large-amplitude vortex structure that differs considerably from what two-dimensional simulations predict. The different vortical configuration leads to more rapid non-linear growth for the fully three-dimensional case, even though the linear growth rate is the same. The increased stratification modifies the interface in a way that might be expected from the two-dimensional results; as the density difference is increased the difference between the bubbles and the spikes becomes more apparent. The up-going fluid rises in relatively large round bubbles, whereas the heavy, down-going fluid falls in thin spikes. The initial perturbations used here are the same as in [39], and lead to symmetric penetration of each fluid into each other for weakly stratified flows.

In the runs discussed above, the viscosity was selected so that the imposed perturbation corresponded to the most unstable wavelength (except in fig. 2b), and the kinematic viscosity of both fluids is the same. Since viscosity obviously has a strong influence on the evolution, it is natural to look at what effect viscosity stratification

Fig. 3. The effect of density stratification on the large amplitude stage of a fully three-dimensional viscous, Rayleigh–Taylor instability. (a) $A = 0.5$, (b) $A = 0.9$. The up-going bubble is bigger, and the down-going spike sharper for the larger stratification.

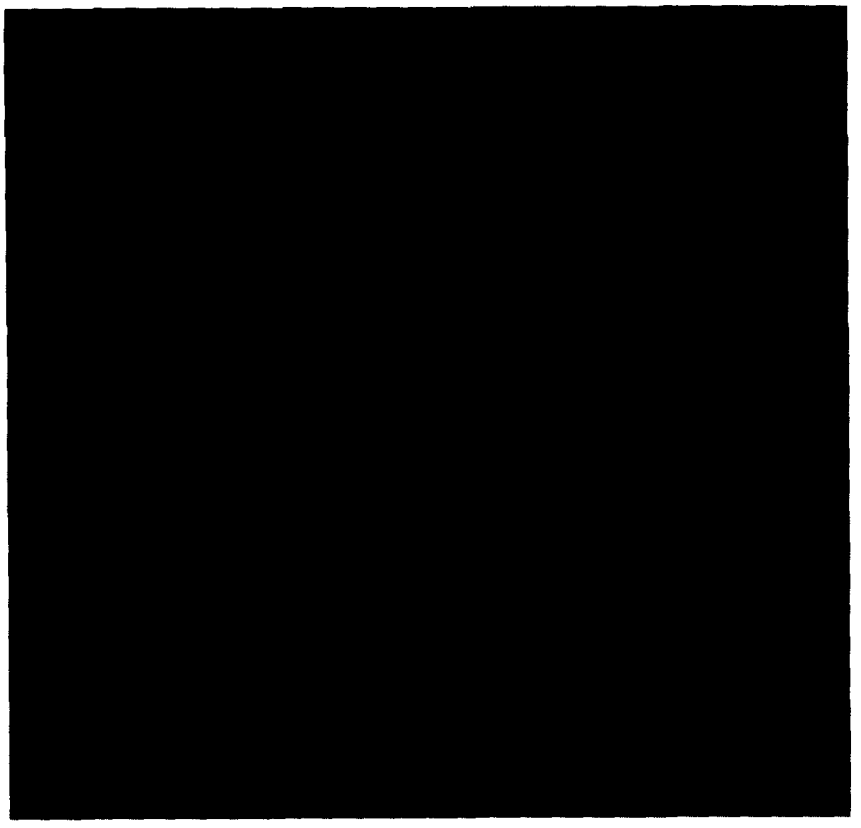

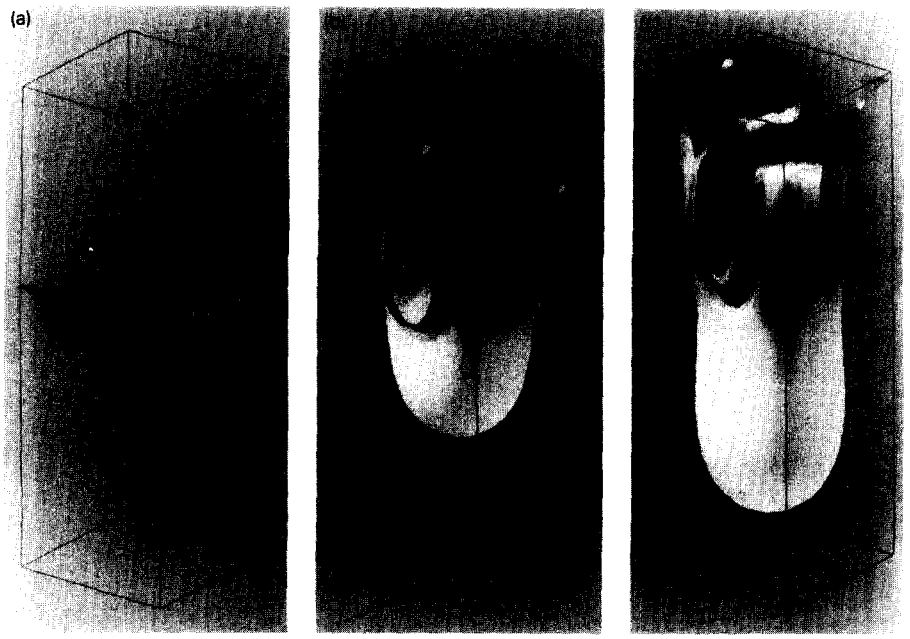

Fig. 4. The effect of viscosity stratification on the evolution of a weakly stratified, three-dimensional Rayleigh–Taylor instability. The bottom fluid is fifty times more viscous than the top fluid.

has. In the run shown in fig. 4, the densities are close (so the evolution would be symmetric if the viscosities were the same), but the bottom fluid is fifty times more viscous than the top one. This result should be compared with the calculations in [39] but may also be compared with the result in fig. 3a, where the asymmetry due to finite density stratification is actually rather small. Obviously there are considerable differences. The low viscosity, top fluid falls down in a large blob, while the more viscous, but lighter, bottom fluid rises in relatively thin fingers. This difference in growth of the fingers and the blobs is also seen in fig. 5, where the amplitude is plotted versus time. The reason for this behavior may be sought by considering how the baroclinic vorticity generated at the interface diffuses into the different fluids. Since vorticity diffuses more easily into the more viscous bottom fluid, the tip of the finger travels faster upward than the tip of the bubble goes downward, and, by continuity, the finger slims down. This behavior has been observed experimentally under creeping flow conditions by Talbot and Jackson [40]. Other simulations, mostly for weak stratification and identical viscosities, suggest that asymmetry may also be induced by the presence of more modes in the initial perturbations, sometimes leading one fluid to "mushroom" into the other, but not vice versa. A systematic study has not been done yet.

We next turn to calculations of colliding bubbles. These calculations have been run for a relatively long time, compared to the calculations of the Rayleigh–Taylor instability and require the continuous restructuring of the interface grid. Surface tension is also included here. Fig. 6 shows two simulations of a collision between two bubbles in a periodic bubble chain. Initially,

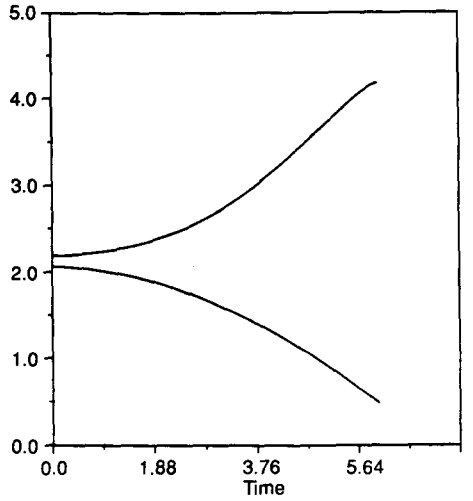

Fig. 5. The vertical position of the tip of the more viscous finger and the less viscous blob, for the run in fig. 4, as a function of non-dimensional time $t\sqrt{Ag/L}$.

two spherical bubbles are at rest in the middle of the computational domain, with their centers two diameters apart in the vertical direction and separated horizontally by a quarter of the diameter. The period in the vertical direction is five times the diameter of the bubbles, and the width of the computational domain in the horizontal directions is half this period. The computational domain is shown at the bottom of each frame. The height of the box is the period of the bubble chain, the left and right boundaries are periodic, and full slip boundaries are implemented in front and back. The bubbles can therefore move out of the original computational domain, and as they do so the bubble pair in the period below moves in. In fig. 6 we, however, follow the original pair. The first bubble pair, inside the box at the bottom, is shown shortly after the run started, and each subsequent pair shows the evolution of the interaction process between the original pair. For an infinite periodic domain, it is necessary to specify either the net volume flux or the total pressure difference across each period. Here we have done the latter and taken the pressure increase from top to bottom equal to the hydrostatic contribution from the fluid mixture.

Bubbles and drops can be characterized by the Eötvös number, Eo, and the Morton number, M, defined as

$$\mathrm{M} = g\mu_o^4/\rho_o\sigma^3, \quad \mathrm{Eo} = \rho_o g d_e^2/\sigma,$$

in addition to the density ratio, ρ_o/ρ_b and the viscosity ratio, μ_o/μ_b. Here, subscript o refers to the outer fluid and b to the bubble fluid. d_e is the diameter of the initially spherical bubble. In the calculations in fig. 6, Eo = 10 and the density ratio is $\rho_o/\rho_b = 40$ in both runs. In (a), $\mathrm{M} = 10^{-2}$ and the viscosity ratio is $\mu_o/\mu_b = 28$, but in (b), $\mathrm{M} = 10^{-3}$ and the viscosity ratio is $\mu_o/\mu_b = 16$. The difference between the runs is, therefore, only the viscosity of the outer fluid (smaller in b). Both calculations are carried out on a 32 by 32 by 64 grid and use about 5000 elements to represent the bubble surface. Surface elements are added and deleted during the run, so the actual number varies.

Initially, the bubbles rise relatively independently of each other and deform towards the steady-state shape of a single bubble in free rise. For this values of the governing parameters the bubbles have a relatively round top and a nearly flat bottom, with the bubbles in the low viscosity fluid in (b) becoming flatter and having a sharper "rim". The top bubble remains more or less of the same shape as the pair rises, but the bottom bubble is accelerated upward and elongated in the strain field induced by the motion of the top bubble. In both runs, the bubbles line up into a nearly axisymmetric configuration. The bottom bubble then accelerates and collides with the top bubble. Both bubbles now become flatter, particularly in the low viscosity fluid (b). After having risen together for a short distance, the top bubble slides to the side, and the the bottom bubble moves toward the side of the top one.

In fig. 7, the vertical coordinate of the centroid of each bubble is plotted versus time, in (a) for the high viscosity outer fluid (6a) and in (b) for the low viscosity outer fluid (6b). Ini-

Fig. 6. Non-axisymmetric merging of two bubbles on a 32 by 32 by 64 grid. Time is non-dimensionalized here by $(\sigma/\rho_o g^3)^{1/4}$. (a) Left two columns. Eo = 10, $M = 10^{-2}$, $\rho_o/\rho_b = 40$, and $\mu_o/\mu_b = 28$. The times shown are: 2.26, 13.58, 22.64, 29.43, 36.22, 43.01, 49.80, 56.59, 63.38 and 69.04. The second column is a continuation of the first one. (b) Right two columns. Eo = 10, $M = 10^{-3}$, $\rho_o/\rho_b = 40$, and $\mu_o/\mu_b = 16$. The times shown are: 2.26, 11.32, 18.11, 22.64, 27.16, 31.69, 36.22, 40.75, 45.27, 49.80, 54.33, 58.85, 63.38 and 67.91. The second column is a continuation of the first one.

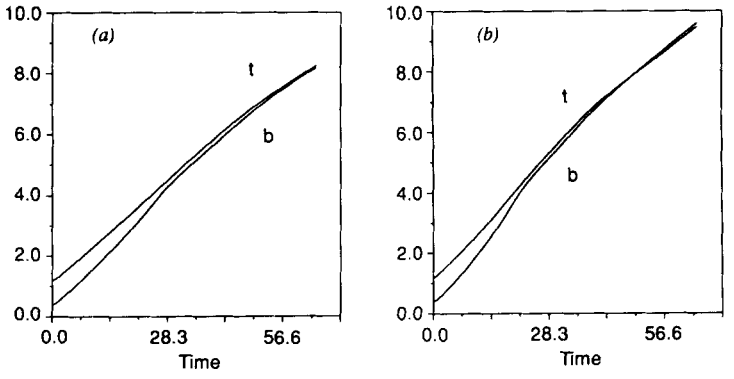

Fig. 7. The vertical position of the center of mass of the bubbles in fig. 6 versus time. Here, t and b denote the bubbles that are initially on the top and bottom, respectively. (a) and (b) as in fig. 6.

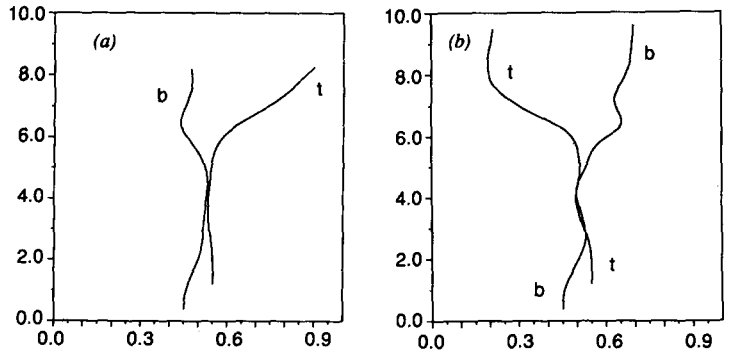

Fig. 8. The path of the center of mass for the bubbles in fig. 6. The vertical scale is one tenth of the horizontal scale. Here, t and b denotes the bubbls that are initiall on the top and bottom, respectively. (a) and (b) as in figs. 6 and 7.

tially, both bubbles move with nearly constant velocity which is slightly larger for the bottom one. The bottom bubble then rises rapidly and collides with the top bubble. The bubble pair accelerates slightly during the collision and then moves with constant velocity for a while. As the bubbles tumble over and start to rise side by side they both slow down. Because the Morton number is smaller, the bubble pair in (b) rises faster and the interaction time is shorter.

Fig. 8 shows the paths of the bubble centroids for the pairs, in the center plane of the box: (a) and (b) are as in figs. 6 and 7. In both cases, the bubbles initially rise straight up but then drift toward the center of the box. The bottom bubble movies more laterally than the top one, in both cases. This motion is slower in the high viscosity fluid and when the bubbles collide, the bottom bubble in the high viscosity fluid is still slightly to the left of the top one as it was initially. In the low viscosity fluid (b), the bottom bubble oveshoots the centerline and then moves back again toward the middle and collides with the top bubble. Although the subsequent evolution similar in that both pairs tumble over and the bottom bubble catches up with the top one, the configuration just before collision makes an important difference: in (a), the top bubble is pushed to the right, but in (b), it goes to the left. Since the bottom bubble in (b) appears to be undergoing oscillatory motion around the centerline as it approaches the top one, it is likely that the post collision motion depends on the phase of this oscillation and thus on the initial separation as well as the viscosity of the outer fluid. As the bottom bubble catches up with the top one, it is bumped slightly outward before it settles down on a trajectory that is nearly parallel with the other bubble. The whole process takes place faster in the low viscosity fluid, as expected. In (a), the bubbles are still not moving parallel at the end of the run, while in (b), it appears that the bubble initially behind has actually passed the other one. Whether the final state consists of a bubble pair rising side by side, or if the bubbles exchange positions and the collision process is repeated, is not yet known.

Both runs are at a relatively high Morton number, and the calculations of Ryskin and Leal [26] suggest that no recirculating wake is present for this parameter values. Fig. 9 shows the velocity field for both pairs after the initial deformation has taken place, but before collision. The velocity field is with respect to a frame of reference moving with the bottom bubble, and no recirculation behind the bubbles is visible. A similar plot in a frame moving with the top bubble is nearly identical. Although a recirculating wake is absent, it is clear that the top bubble shields the bottom one from the oncoming flow and that the momentum defect in the wake of the top bubble causes the upward acceleration of the bottom

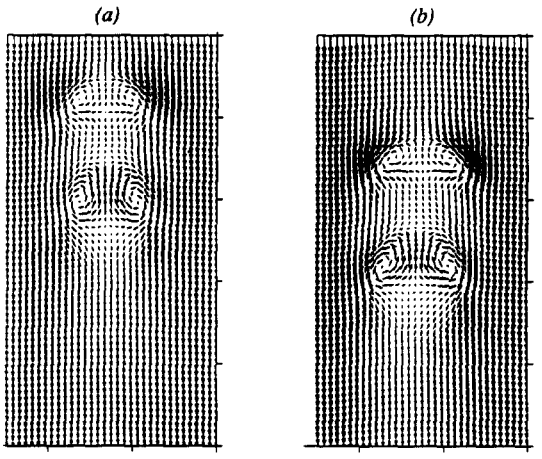

Fig. 9. The velocity field due to the bubbles in fig. 6 before the bubbles collide. (a) and (b) as in figs. 6–8.

one.

We note that for calculations that involve complicated interactions such as these and that consist of thousands of time steps, it is likely that a higher order time integration, than the first order used here, would improve the results. Nevertheless, we believe that the calculations are reasonably accurate and correctly represent the physical processes simulated. In two-dimension, similar calculations have been checked extensively by grid refinement, and those tests suggest that the resolution used there is sufficient in the parameter range simulated. Consultation with experimental results [34] also suggests good agreement but different setup and uncertainties about contamination effects call for a more detailed study. We have also found good qualitative agreement with the axisymmetric, steady-state calculations of Ryskin and Leal [26] and Dandy and Leal [27]. A direct comparison is, however, not possible with our current setup. Our bubbles are confined to a rather small domain but Leal and coworkers could afford a much larger domain for their axisymmetric computations.

4. Conclusions

Full numerical simulations of multi-fluid flows are discussed and examples of the Rayleigh–Taylor instability and bubble motion are presented. These preliminary results, as well as results presented elsewhere, suggest that full simulations of relatively complicated multi-fluid systems are well within reach.

Full simulations will, naturally, always be limited to somewhat modest-sized systems. Our experience suggests that for a high viscosity and surface tension a meaningful resolution of a single bubble can be achieved on as little as a 16^3 grid. A simulation on a 64^3 or even 128^3 grid would be able to include several bubbles. Nevertheless, a full simulation of most mixing processes is obviously as much out of the question as full simulations of a realistic turbulent flow. The utility of full simulations is in developing an insight into the basic micromechanisms, much as analytical solutions do when they are obtainable. In addition to information about the bubble motion itself – some of which may be obtained more easily experimentally, such as shapes and interactions – full simulations allow examination of quantities that are difficult to measure, such as the velocity field, as well as direct evaluation of macroscopic quantities controlled by the microscopic motion, such as how fluxes of mass and momentum depend on the bubble configuration. In addition to complementing experiments in providing a fundamental insight, full simulations are therefore of great utility for analytical modeling, both on the microscopic and macroscopic levels.

Acknowledgements

Discussions with Professors G. Brereton and H. Merte are acknowledged. This work was supported by NSF Grant No. MSM87-07646 and by a grant from the Phoenix Memorial Foundation at the University of Michigan. The calculations

were done on the computers at the San Diego Supercomputer Center, which is sponsored by the NSF.

References

[1] J.M. Ottino, Phys. Fluids A 3 (1991) 1417.
[2] S.O. Unverdi and G. Tryggvason, J. Comput. Phys. 100 (1991) 25.
[3] B.J. Daly, Phys. Fluids 10 (1967) 297; J. Comput. Phys. 4 (1969) 97.
[4] D.H. Sharp, Physica D 12 (1984) 3.
[5] G. Tryggvason, J. Comput. Phys. 75 (1988) 253.
[6] J.A. Zufiria, Phys. Fluids 31 (1988) 3199.
[7] J. Glimm, O. McBryan, R. Menikoff and D.H. Sharp, SIAM J. Sci. Stat. Comput. 7 (1987) 230.
[8] S.G. Yiantsios and B.G. Higgins, Phys. Fluids A 1 (1989) 1484.
[9] J. Glimm, X.L. Li, R. Menikoff, D.H. Sharp and Q. Zhang, Phys. Fluids A 2 (1990) 2046.
[10] D.L. Youngs, Phys. Fluids A 3 (1991) 1312.
[11] R. Clift, J.R. Grace and M.E. Weber, Bubbles, Drops and Particles (Academic Press, New York, 1978).
[12] S.W. Churchill, Viscous flows. The Practical Use of Theory (Butterworth, 1988).
[13] G. Hetsroni (ed.). Handbook of multiphase systems (Hemisphere, 1982).
[14] J.F. Harper, Adv. Appl. Mech. 12 (1972) 59.
[15] P.P. Wegener and J.-Y. Parlange, Ann. Rev. Fluid Mech. 5 (1976) 79.
[16] J.M. Rallison, Ann. Rev. Fluid Mech. 16 (1984) 45.
[17] A. Acrivos, Ann. NY Acad. Sci. 404 (1983) 1; in: Physicochemical Hydrodynamics, Interfacial Phenomena, ed. M.G. Velarde, Vol. 1 (Plenum, New York, 1987).
[18] G.K. Youngren and A. Acrivos, J. Fluid Mech. 76 (1976) 433.
[19] J.M. Rallison, J. Fluid Mech. 109 (1981), 465.
[20] H.A. Stone and L.G. Leal, J. Fluid Mech. 198 (1989) 333.
[21] C.J. Koh and L.G. Leal, Phys. Fluids A 1 (1989) 1309.
[22] C. Pozrikidis, J. Fluid Mech. 210 (1990) 1.
[23] B.K. Chi and L.G. Leal, J. Fluid Mech. 201 (1989) 123.
[24] M.J. Martinez and K.S. Udell, J. Fluid Mech. 210 (1990) 565.
[25] H.A. Stone and L.G. Leal, Phys. Fluids A 3 (1991).
[26] G. Ryskin and L.G. Leal, J. Fluid Mech. 148 (1984) 1; 148 (1984) 19; 148 (1984) 37.
[27] D.S. Dandy and L.G. Leal, J. Fluid Mech. 208 (1989) 161.
[28] C.R. Anderson, J. Comput. Phys. 61 (1985) 417.
[29] G.R. Baker and D.W. Moore, Phys. Fluids A 1 (1989) 1451.
[30] D.E. Fyfe, E.S. Oran and M.J. Fritts, J. Comput. Phys. 76 (1988) 349.
[31] S.H. Brecht and J.R. Ferrante, Phys. Fluids A 1 (1989) 1166.
[32] G.L. Chahine, in: Numerical Methods for Multiphase Flows, eds. Celik, Hughes, Crowe and Lankford (ASME, New York, 1990) p. 57.
[33] J.F. Davidson, R. Clift and D. Harrison, eds., Fluidization, 2nd. ed. (Academic Press, 1985).
[34] R. Clift and J.R. Grace, Chem. Eng. Prog., Symp. Ser. 14 66;
N. de Nevers and J.-L. Wu, AIChE J. 17 (1971) 182; S. Narayanan, L.H. Goossens and N.W.F. Kossen, Chem. Eng. Science 29 (1974) 2071;
D. Bhaga and M.E. Weber. Chem. Eng. Science 35 (1980) 2467;
D. Dekee, P.J. Carreau and J. Mordarski, Chem. Eng. Science 41 (1986) 2273.
[35] J.P. Boris, Ann. Rev. Fluid Mech. 21 (1989) 345.
[36] C.S. Peskin, J. Comput. Phys 25 (1977) 220;
L.J. Fauci and C.S. Peskin, J. Comput. Phys. 77 (1988) 80;
A.L. Fogelson and C.S. Peskin, J. Comput. Phys. 79 (1988) 50.
[37] C.W. Hirt and B.D. Nichols, J. Comput. Phys. 39 (1981) 201;
J.M. Hyman, Physica D 12 (1984) 396;
E.S. Orain and J.P. Boris, Numerical simulations of reactive Flow (Elsevier, Amsterdam, 1987);
J.M. Floryan and H Rasmussen, Appl. Mech. Rev. 42 (1989) 323.
[38] P.H. Todd and R.J.Y. McLeod, Computer-aided design 18 (1986) 33.
[39] G. Tryggvason and S.O. Unverdi, Phys. Fluids A 2 (1990) 656.
[40] C.J. Talbot and M.P.A. Jackson, Sci. Am. 257 (1987) 70.